S-glutathionylation activates STIM1 and alters mitochondrial homeostasis

Brian J. Hawkins,[1] Krishna M. Irrinki,[1] Karthik Mallilankaraman,[1] Yu-Chin Lien,[2] Youjun Wang,[1] Cunnigaiper D. Bhanumathy,[3] Ramasamy Subbiah,[1] Michael F. Ritchie,[1] Jonathan Soboloff,[1] Yoshihiro Baba,[4] Tomohiro Kurosaki,[4] Suresh K. Joseph,[3] Donald L. Gill,[1] and Muniswamy Madesh[1]

[1]Department of Biochemistry, Temple University, Philadelphia, PA 19140
[2]Institute for Environmental Medicine, University of Pennsylvania, Philadelphia, PA 19104
[3]Department of Pathology, Anatomy, and Cell Biology, Thomas Jefferson University, Philadelphia, PA 19107
[4]Laboratory of Lymphocyte Differentiation, World Premiere International Immunology Frontier Research Center, Osaka University, Osaka 565-0871, Japan

Oxidant stress influences many cellular processes, including cell growth, differentiation, and cell death. A well-recognized link between these processes and oxidant stress is via alterations in Ca^{2+} signaling. However, precisely how oxidants influence Ca^{2+} signaling remains unclear. Oxidant stress led to a phenotypic shift in Ca^{2+} mobilization from an oscillatory to a sustained elevated pattern via calcium release–activated calcium (CRAC)–mediated capacitive Ca^{2+} entry, and stromal interaction molecule 1 (STIM1)– and Orai1-deficient cells are resistant to oxidant stress. Functionally, oxidant-induced Ca^{2+} entry alters mitochondrial Ca^{2+} handling and bioenergetics and triggers cell death. STIM1 is S-glutathionylated at cysteine 56 in response to oxidant stress and evokes constitutive Ca^{2+} entry independent of intracellular Ca^{2+} stores. These experiments reveal that cysteine 56 is a sensor for oxidant-dependent activation of STIM1 and demonstrate a molecular link between oxidant stress and Ca^{2+} signaling via the CRAC channel.

Introduction

Calcium is a ubiquitous second messenger that is tightly controlled inside the ER, where it can be rapidly mobilized to translate receptor-mediated signaling into a cellular response. After the initial receptor-initiated Ca^{2+} transient, a sustained Ca^{2+} influx from the extracellular milieu occurs that serves to provide prolonged Ca^{2+} signals and allow ER store refilling to permit subsequent signaling events (Berridge et al., 2003; Parekh and Putney, 2005; Feske, 2007; Deng et al., 2009). Activation of this capacitive Ca^{2+} entry by the calcium release–activated calcium (CRAC) channel involves a complex molecular choreography. In general, a decrease in ER luminal Ca^{2+} triggers Ca^{2+} dissociation from the ER-resident protein STIM1 (stromal interaction molecule 1), which oligomerizes and translocates into discrete junctions near the plasma membrane, where it binds to and activates members of the Orai family of CRAC channels (Luik et al., 2006; Prakriya et al., 2006; Vig et al., 2006; Yeromin et al., 2006; Smyth et al., 2007; Park et al., 2009; Yuan et al., 2009). In addition to buffering Ca^{2+} released from ER stores, mitochondria are also intimately involved in CRAC activation. Through their associations with the ER (Rizzuto et al., 1998; Csordás et al., 2006), mitochondrial Ca^{2+} buffering can enhance ER Ca^{2+} depletion and, thus, increase CRAC activation (Gilabert et al., 2001). Furthermore, mitochondrial Ca^{2+} release can enhance ER Ca^{2+} refilling and, thus, reduce the duration of CRAC channel activation (Parekh, 2008). Mitochondrial Ca^{2+} uptake also stimulates the production of reactive oxygen species (ROS), which can influence both ER Ca^{2+} release (Bootman et al., 1992; Huddleston et al., 2008) and reuptake by the ER (Kaplan et al., 2003; Ihara et al., 2005). A prominent posttranslational molecular target of ROS is protein cysteine residues, which reversibly form disulfide bridges or sulphenic acid (PSOH) or irreversibly

Correspondence to Donald L. Gill: dgill@temple.edu; or Muniswamy Madesh: madeshm@temple.edu

Abbreviations used in this paper: BHA, butylated hydroxyanisole; BSO, buthionine sulfoximine; CRAC, calcium release–activated calcium; DCF, dichlorofluorescein; DM, double mutant; ECM, extracellular medium; GSH, glutathione; HE, dihydroethidine; KO, knockout; LPS, lipopolysaccharide; MALDI, matrix-assisted laser desorption/ionization; MCB, monochlorobimane; MEF, mouse embryonic fibroblast; ROS, reactive oxygen species; Tg, thapsigargin; TMRE, tetramethylrhodamine, ethyl ester; WT, wild type.

The Rockefeller University Press $30.00
J. Cell Biol. Vol. 190 No. 3 391–405
www.jcb.org/cgi/doi/10.1083/jcb.201004152

produce sulphinic (PSO_2H) or sulphonic acid (PSO_3H) moieties (Veal et al., 2007). Additionally, a common modification of protein thiol is S-glutathionylation via the reversible reaction between protein cysteine residues and glutathione (GSH; Anathy et al., 2009; Dalle-Donne et al., 2009). However, the specific molecular targets of oxidants that affect Ca^{2+} signaling and mitochondrial function are not fully defined. In this study, we demonstrate that, in addition to being a sensor for intracellular Ca^{2+} stores, STIM1 functions as a redox sensor to constitutively activate CRAC channels under oxidative conditions. S-glutathionylation or $C^{56}A$ mutation of STIM1 positively regulates CRAC channel activation, which leads to mitochondrial Ca^{2+} overload and alterations in cellular bioenergetics. Importantly, we find that GSH is a critical regulator of STIM1 signaling during oxidative stress.

Results

Oxidative stress shapes calcium signaling patterns by depleting cellular GSH

To investigate the role of oxidant stress in Ca^{2+} homeostasis, DT40 B-lymphocytes were challenged with lipopolysaccharide (LPS), a component of the gram-negative bacterial cell wall that stimulates ROS production through the Toll-like receptor 4 (Asehnoune et al., 2004; Madesh et al., 2005). 1 µg/ml LPS evoked a time-dependent increase in cellular oxidative stress that peaked at 5 h and could be ablated by 100 µM of the antioxidant butylated hydroxyanisole (BHA; Fig. 1, A and B). In nonchallenged B cells, αIgM activation (1.5 µg/ml) of the B cell receptor stimulates robust Ca^{2+} mobilization that presented as a nonsynchronized oscillatory pattern (individual traces) and rapidly returned to baseline (Fig. 1 C, dashed line). In contrast, 5 h of LPS treatment resulted in a phenotypic shift toward a more elevated Ca^{2+} oscillation pattern after αIgM addition that remained elevated above baseline (Fig. 1 D). Restoration of an oscillatory Ca^{2+} signaling pattern could be accomplished by scavenging ROS with BHA (Fig. 1 E), indicating that the effect of LPS on Ca^{2+} signaling may be mediated by oxidants. Cells pretreated with 100 µM hydrogen peroxide (H_2O_2) for 20 min also resulted in a sustained Ca^{2+} mobilization pattern, although to a much higher degree than the LPS and with no oscillations observed (Fig. 1 F). In normal cells, oxidants are effectively scavenged through multiple endogenous antioxidants, including superoxide dismutase, catalase, and GSH peroxidase. In addition, the tripeptide GSH, composed of the amino acids γ-glutamic acid, cysteine, and glycine, is present in millimolar quantities in cells and serves as an important antioxidant and redox molecule. As expected, LPS led to a time-dependent depletion of the cellular GSH pool, as determined by the GSH cross-linking fluorophore monochlorobimane (MCB; Fig. 1 G) and by direct measurement of cellular GSH (unpublished data). Similar to BHA, GSH replenishment with cell-permeable GSH-ester restored Ca^{2+} oscillations in LPS-challenged DT40 cells in response to αIgM (Fig. 1 H). Furthermore, GSH efflux was unaltered in cells challenged with LPS, indicating a reduction in intracellular GSH levels rather than loss of GSH to the extracellular milieu (unpublished data).

Loss of GSH and sustained cytosolic calcium alter mitochondrial calcium handling

Under normal physiological conditions, Ca^{2+} is efficiently taken up and released by mitochondria in concert with cytosolic Ca^{2+} levels (Fig. 2, A and B). However, the sustained elevation of cytosolic Ca^{2+} concentration mediated by oxidative stress (1 µg/ml LPS for 5 h) dramatically enhances mitochondrial Ca^{2+} uptake (Fig. 2, C and D). Interestingly, elevated mitochondrial Ca^{2+} uptake did not occur immediately after αIgM stimulation but, rather, increased incrementally over time. This observation indicates that during oxidative stress, mitochondrial Ca^{2+} uptake is tied not to the magnitude of the cytosolic Ca^{2+} levels but to the diastolic Ca^{2+} level between oscillatory peaks. In addition to ROS production, LPS targets multiple signaling cascades, including the activation of NF-κB and the production of various cytokines, which may also impact the Ca^{2+} mobilization pattern and must be considered. As supplementation of GSH restored Ca^{2+} oscillations in LPS-challenged cells (Fig. 1 H), we chose to focus on GSH to dissect the specific role of oxidants in modulating physiological Ca^{2+} signaling.

To induce oxidative stress secondary to a depletion of GSH, DT40 cells were treated with 200 µM of the chemosensitizing agent buthionine sulfoximine (BSO; for 24 h), which inhibits γ-glutamyl synthetase, the rate-limiting enzyme in GSH synthesis (Arrick et al., 1981; Madesh et al., 1998; Diehn et al., 2009). In contrast to untreated conditions, GSH depletion by BSO resulted in a dramatic alteration in the Ca^{2+} signaling phenotype from an oscillatory to a more sustained Ca^{2+} mobilization pattern after αIgM addition (Fig. 2 E). Furthermore, mitochondrial Ca^{2+} handling in BSO-treated cells was similar to that of DT40 cells treated with LPS (Fig. 2, F and G) and was proportional to the degree of GSH depletion (Fig. S1). To delineate whether the Ca^{2+} handling evoked by BSO was attributable to GSH depletion (Fig. 2, H–K), we next assessed the coordination between cytosolic and mitochondrial Ca^{2+}. In contrast to untreated conditions (Fig. 2 L), BSO challenge triggered sustained mitochondrial Ca^{2+} uptake (Fig. 2 M) that could be reversed by GSH supplementation (Fig. 2 N). Similarly, supplementation of the antioxidants BHA or GSH-ester restored the oscillatory mitochondrial Ca^{2+}-handling pattern in LPS-treated cells (unpublished data). These results suggest two important points: (1) the effects of LPS on cytosolic and mitochondrial Ca^{2+} handling are mediated through GSH oxidation and (2) BSO constitutes a physiologically relevant model in which to study the effects of oxidant stress on cellular Ca^{2+} signaling.

Altered calcium signaling during oxidant stress is mediated through the CRAC channel

A plausible explanation for the elevation in diastolic Ca^{2+} between oscillatory peaks may be an influx of Ca^{2+} from the extracellular milieu via activation of the CRAC channel. The absence of extracellular Ca^{2+} did not affect the αIgM response in wild-type (WT) DT40 cells but stimulated robust Ca^{2+} entry upon the addition of 2 mM Ca^{2+} (Fig. 3 A). Interestingly, the BSO-mediated Ca^{2+}

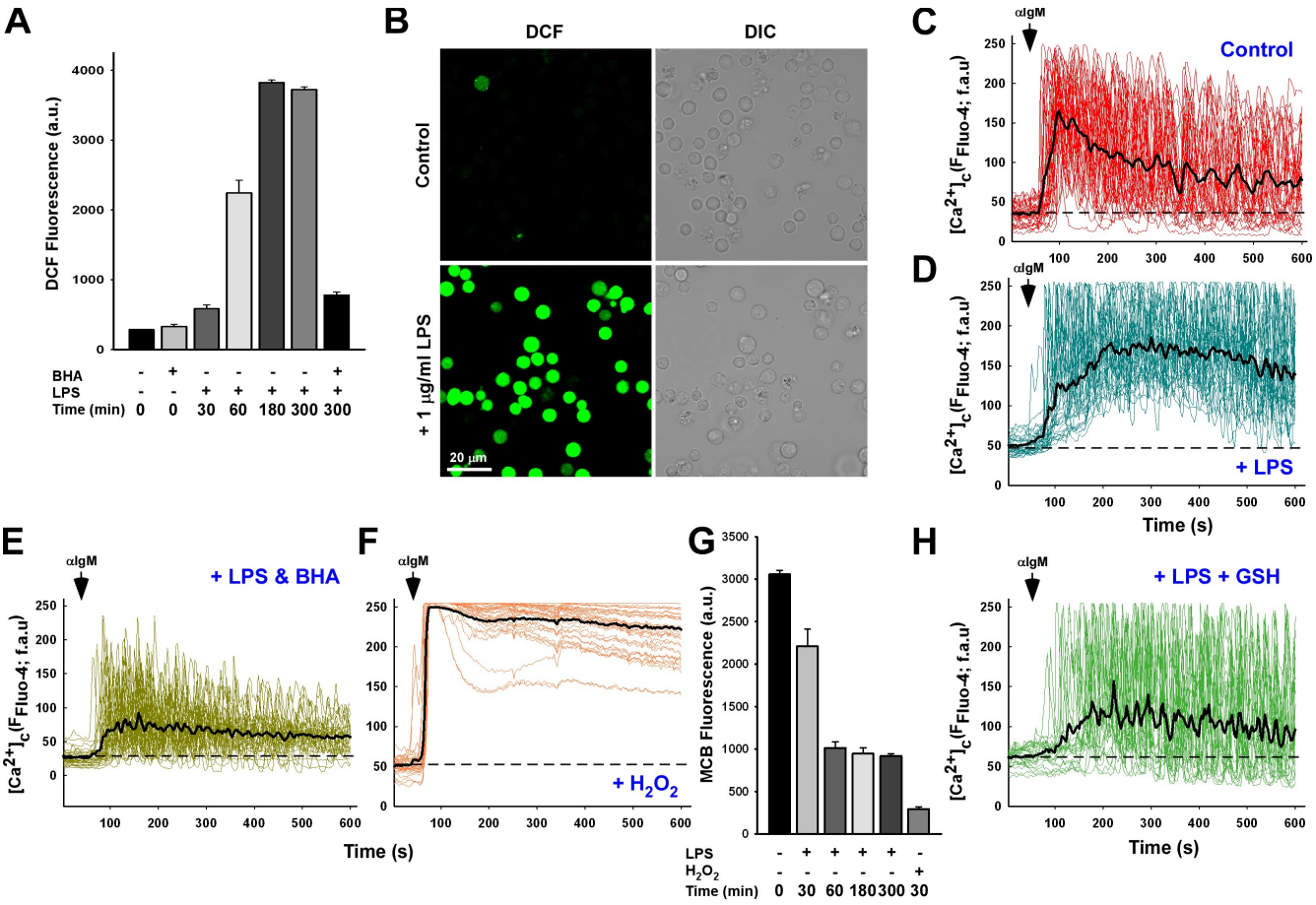

Figure 1. **LPS-induced oxidative stress alters B cell receptor calcium signaling via the depletion of cellular GSH.** (A) DT40 cells loaded with ROS indicator H_2DCF-DA were challenged with 1 µg/ml LPS for the indicated time period and DCF fluorescence (arbitrary units [au]) measured to assess cellular oxidants either in the absence or presence of 100 µM of the antioxidant compound BHA. Values are representative of three independent experiments. (B) Representative images of DCF fluorescence in DT40 cells in response to 5-h LPS. DIC, differential interference contrast. (C and D) DT40 cells loaded with Fluo-4 were activated by addition of 1.5 µg/ml αIgM and fluorescence recorded via confocal microscopy in control cells (C; n = 33) and after a 5-h 1 µg/ml LPS treatment (D; n = 33). fau, fluorescence arbitrary units. Black traces are mean values of all traces, and baseline fluorescence is indicated as dashed lines. (E) DT40 cells were pretreated with 100 µM BHA before addition of LPS (n = 33). (F) αIgM evoked Ca^{2+} mobilization in response to direct oxidant challenge with 100 µM H_2O_2 for 20 min (n = 34). (G) DT40 cells activated with either LPS or H_2O_2 were loaded with the GSH cross-linking fluorophore MCB to assess reduced GSH levels via the GSH-MCB conjugate. (H) Calcium mobilization after αIgM addition in DT40 cells challenged with LPS and supplemented with 2.5 mM cell-permeable GSH-ester. αIgM addition is noted by arrows. Error bars indicate mean ± SEM.

phenotype (Fig. 3 B) could be normalized by removing extracellular Ca^{2+} (Fig. 3 C). Like untreated cells, reintroduction of extracellular Ca^{2+} in BSO-treated DT40 cells resulted in CRAC activation, which is mediated by the ER-resident protein STIM1 (Liou et al., 2005; Roos et al., 2005). DT40 cells lacking STIM1 responded in a similar manner to WT cells in response to αIgM. However, unlike WT cells, STIM1 knockout (KO) cells fail to demonstrate capacitive Ca^{2+} entry upon store depletion (Fig. 3 D; Baba et al., 2006). Although DT40 cells express both STIM1 and STIM2, the role of STIM2 in IgM-mediated Ca^{2+} entry is less clear. Surprisingly, BSO challenge did not alter the Ca^{2+} mobilization pattern in STIM1-deficient DT40 cells either in the presence (Fig. 3 E) or absence (Fig. 3 F) of extracellular Ca^{2+}, despite a near-complete depletion of cellular GSH levels (Fig. 3 H). We next chose to determine whether the sustained Ca^{2+} elevation pattern during oxidative stress requires Orai molecules, which are the plasma membrane pore-forming units of the CRAC channel. Elimination of Orai1 and -2 evoked an oscillatory Ca^{2+} mobilization pattern during oxidative stress (Fig. 3 G) that appears to be Orai1 dependent (Fig. S2), further verifying CRAC activation during BSO-induced oxidative stress. Oxidative stress did not alter expression of the plasma membrane Ca^{2+} ATPases (PMCA1/4), nor did it affect cellular ATP levels (unpublished data), further verifying activation of the CRAC channel and not ablated extrusion of Ca^{2+} from the cytosol.

Depletion of GSH is associated with an elevation in ROS production (Armstrong and Jones, 2002). However, only a slight increase in superoxide generation (the initial radical species) was observed in WT DT40 cells after addition of BSO, as detected by the superoxide indicator dye dihydroethidine (HE; Fig. 3 I). Superoxide anions will undergo reduction either spontaneously or enzymatically in the presence of superoxide dismutase to form the stable oxidant H_2O_2. Unlike superoxide, BSO challenge elicited a dramatic increase in H_2O_2 in WT DT40 cells, as detected by the general ROS indicator dichlorofluorescein (DCF), indicative of a cellular deficiency in H_2O_2 scavenging (Fig. 3 J). However, only a smaller increase in H_2O_2 was observed in STIM1 KO DT40 cells (Fig. 3 J), suggesting that loss of STIM1 attenuates H_2O_2 accumulation. Importantly, BSO-mediated ROS accumulation was not

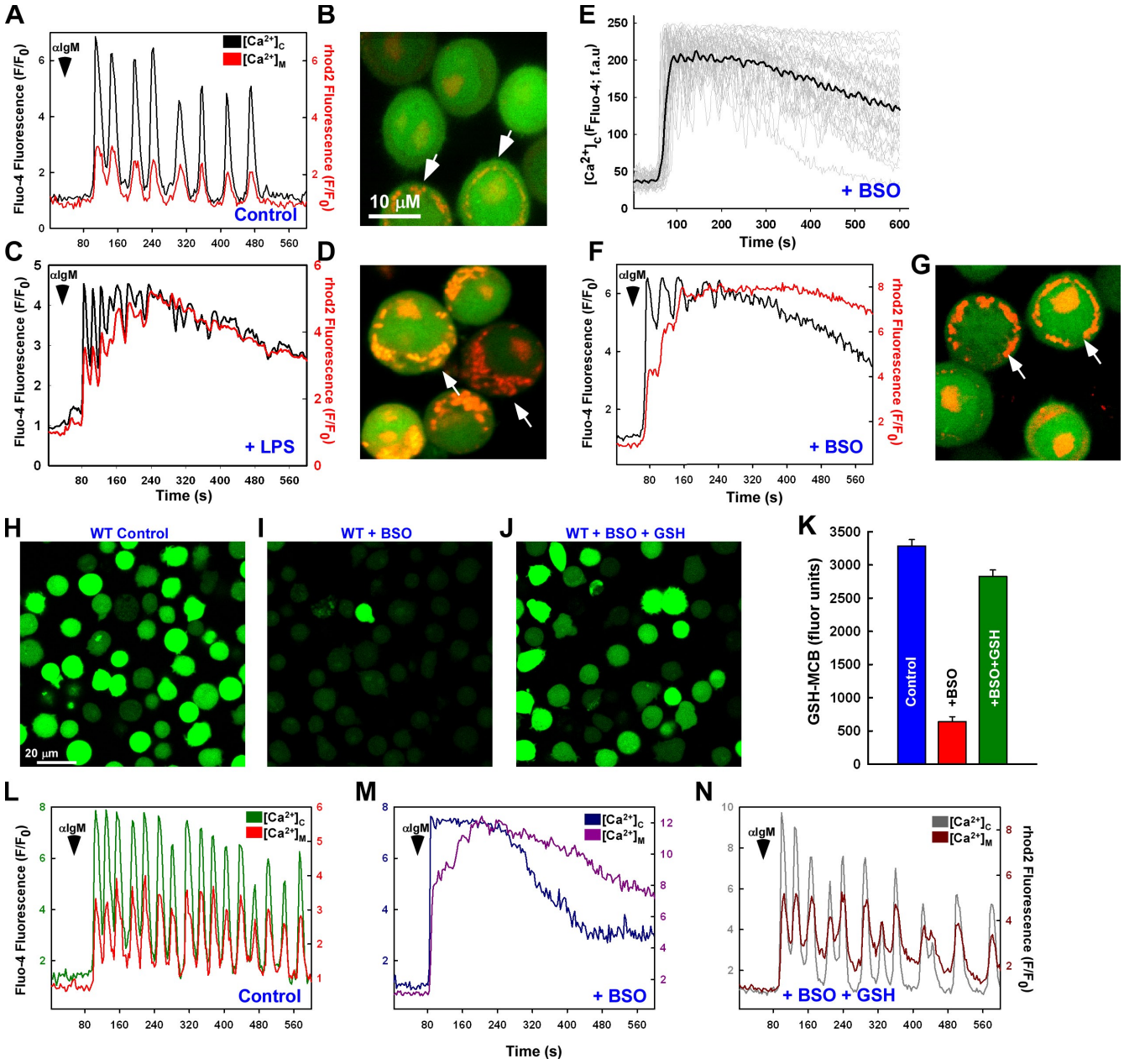

Figure 2. **GSH depletion elicits alterations in mitochondrial calcium handling.** DT40 cells were loaded with Fluo-4 and rhod-2 to simultaneously visualize cytosolic and mitochondrial Ca^{2+}, respectively. (A–D) Representative baseline normalized fluorescence changes (F/F_0) and images of a single cell after 1.5 μg/ml αIgM addition in control (A and B) and 1 μg/ml LPS-challenged (C and D; 5 h) cells. (B and D) Arrows indicate mitochondrial Ca^{2+} levels as detected by rhod-2 fluorescence. (E) αIgM-induced Ca^{2+} mobilization (Fluo-4 fluorescence arbitrary units [fau]) in individual DT40 cells exposed to 200 μM of the GSH synthesis inhibitor BSO for 24 h (n = 37). Black trace is the mean value of all cells. (F and G) Representative baseline normalized fluorescence changes of cytosolic (Fluo-4) and mitochondrial (rhod-2) Ca^{2+} and images of a single cell after 1.5 μg/ml αIgM addition in 200 μM BSO-treated cells (24 h). (G) Arrows indicate mitochondrial Ca^{2+} levels as detected by rhod-2 fluorescence. (H–J) Representative images of the MCB-GSH conjugate in control (H), BSO-treated cells (I), or BSO-treated cells supplemented with 2.5 mM GSH (J) via confocal microscopy. (K) Data for different conditions were measured from six independent experiments (n = 6). (L–N) Representative fluorescence changes of the cytosolic and mitochondrial Ca^{2+} changes in a single cell after αIgM addition in control (L), BSO-treated (M), and BSO + GSH-ester–challenged (N) cells of five independent experiments. αIgM addition is noted by arrowheads. Error bars indicate mean ± SEM.

altered in the presence of 30 μM of the plasma membrane NADPH oxidase inhibitor diphenyleneiodonium (Fig. 3 K), excluding the possibility that BSO enhanced oxidant generation via NADPH oxidase. This important finding reveals two key features of Ca^{2+} signaling during oxidative stress: (1) either STIM1 or Orai1 are a potential target of oxidative stress, and (2) activation of the CRAC channel can be regulated by cellular redox status.

STIM1-mediated calcium entry is required for sustained mitochondrial calcium uptake and aberrant bioenergetics

B cell receptor cross-linking results in coordinated cytosolic Ca^{2+} mobilization and mitochondrial Ca^{2+} uptake in both WT (Fig. 4 A, top) and STIM1 KO cells (Fig. 4 A, bottom). The coordination between cytosolic Ca^{2+} mobilization and mitochondrial

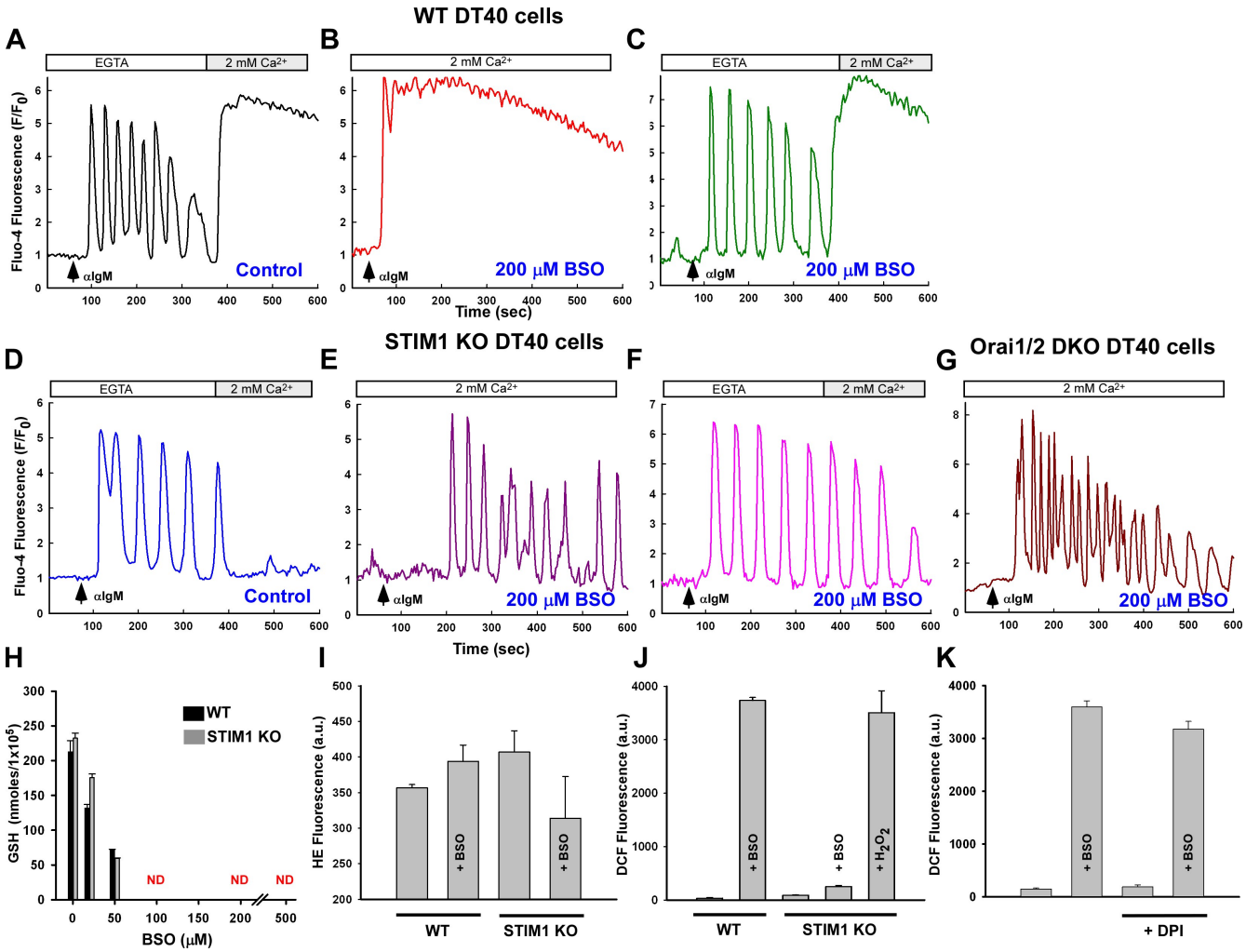

Figure 3. **Loss of the CRAC channel retains the Ca^{2+} oscillation phenotype during oxidative stress.** DT40 cells were loaded with Fluo-4 and Ca^{2+} mobilization recorded after αIgM addition. Traces are representative of the typical cellular response. (A) Capacitive Ca^{2+} entry after αIgM mobilization. (B) Oxidative stress alters the Ca^{2+} mobilization pattern in WT DT40 cells. (C) Ca^{2+} oscillations can be restored by removal of extracellular Ca^{2+} (200 μM EGTA). (D) Ca^{2+} mobilization pattern in STIM1 KO DT40 cells is similar to WT but lack subsequent capacitive Ca^{2+} entry and is resistant to BSO challenge both in the presence (E) and absence (F) of extracellular Ca^{2+}. (n = 6) (G) αIgM-evoked Ca^{2+} mobilization in Orai1/2 DKO cells are similar to STIM1 KO cells. (H)Total GSH levels as determined by luminol fluorescence in response to increasing concentrations of BSO for 24 h. (I) Superoxide anion production in DT40 cells as detected by hydroethidine fluorescence (HE) via confocal microscopy (n = 3). (J) Presence of the superoxide anion degradation product H_2O_2 via DCF fluorescence via confocal microscopy from three independent experiments (n = 3). 1 mM H_2O_2 was added to BSO-challenged STIM1 KO DT40 cells for 30 min as a positive control. (K) DCF fluorescence in WT DT40 cells in the presence of the NADPH oxidase inhibitor diphenyleneiodonium (DPI; 30 μM) after 20 h of BSO challenge. ND, nondetectable. Error bars indicate mean ± SEM.

Ca^{2+} uptake can be attributed to the close physical proximity between the mitochondria and the ER (Filippin et al., 2003). A previous study showed that mitochondria may in fact be tethered to the ER and that this tethering is important in both physiological and pathological signaling (Pinton et al., 2008). Our current findings suggest that it is Ca^{2+} from the extracellular milieu and the resultant elevation in diastolic Ca^{2+} between oscillatory peaks (i.e., temporal Ca^{2+} increase) that are key determinants of sustained mitochondrial Ca^{2+} uptake during oxidative stress (Fig. S3, A and B). Although BSO challenge dramatically altered mitochondrial Ca^{2+} uptake in WT cells (Fig. 4, B and C, top), STIM1 KO cells did not exhibit sustained mitochondrial Ca^{2+} uptake in response to αIgM (Fig. 4, B and C, bottom) even after reintroduction of extracellular Ca^{2+} (Fig. S3 C).

Sustained cytosolic Ca^{2+} or aberrant mitochondrial Ca^{2+} uptake will lead to irreversible mitochondrial dysfunction and bioenergetic collapse (Crompton, 1999; Duchen, 2000). Consistent with our findings that BSO challenge leads to sustained mitochondrial Ca^{2+} uptake (Fig. 4 C), BSO-pretreated WT DT40 cells consumed less oxygen after the sequential additions of the mitochondrial complex I substrates malate and pyruvate and the complex II/III substrate succinate compared with nontreated cells (Fig. 4 D). In contrast, BSO treatment did not affect oxygen consumption in STIM1 KO DT40 cells. Ultimately, this reduction in mitochondrial bioenergetics will decrease mitochondrial energy production and result in cell death. As reported previously (Takata et al., 1995; White et al., 2005), chronic αIgM challenge induced Ca^{2+}-mediated cell death in WT DT40 cells that was markedly enhanced by BSO challenge at all time points

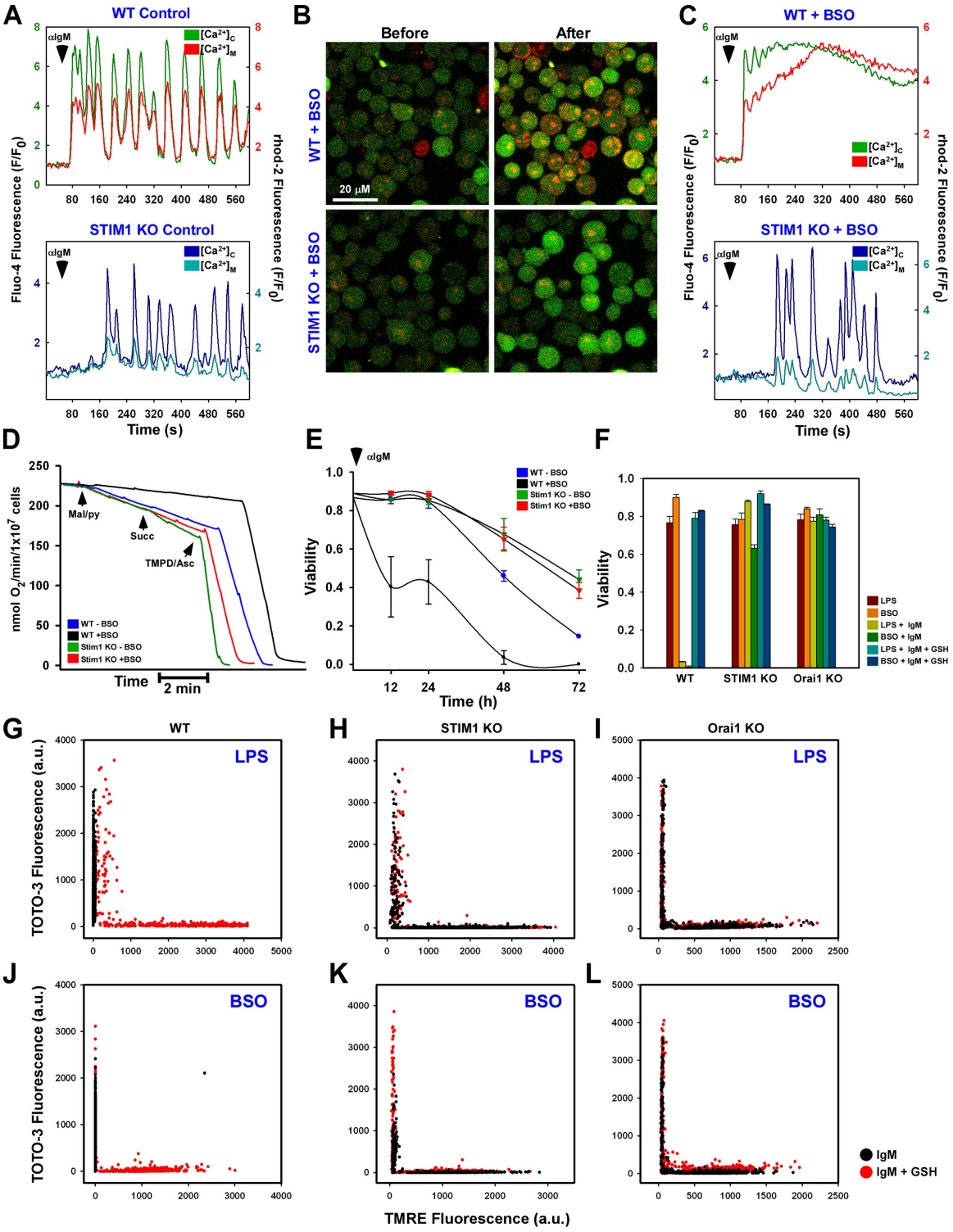

Figure 4. **The CRAC channel is requisite for oxidative stress-induced alterations in mitochondrial Ca^{2+} handling, bioenergetics, and cell death.** Fluo-4– and rhod-2–loaded DT40 cells were stimulated with αIgM and fluorescence changes recorded via confocal microscopy. (A) Coordinated cytosolic and mitochondrial Ca^{2+} levels in control DT40 cells. (B) Confocal images before and after αIgM addition in BSO-pretreated WT (top) and STIM1 KO (bottom) cells. (C) Representative single-cell traces of cytosolic and mitochondrial Ca^{2+} levels after αIgM stimulation in BSO-treated DT40 cells. (D) Oxygen consumption in DT40 cells in response to complex I (malate/pyruvate), complex II/III (succinate), and complex IV (TMPD/ascorbate) substrates. Traces are representative of at least five independent experiments. (E) Sensitization of DT40 cells to 1.5 µg/ml αIgM-induced cell death by BSO, as determined by nuclear incorporation of TOTO-3. αIgM was added to cells every 24 h. Values were determined by counting TOTO-3–positive cells in five independent fields at the indicated time points via confocal microscopy ($n = 3$). (F) DT40 cells were sensitized with either 1 µg/ml LPS for 5 h or 200 µM BSO for 24 h and treated with 1.5 µg/ml αIgM for 48 h either in the absence or presence of 2.5 mM GSH. Cell viability was assessed as the percentage of TOTO-3–negative cells in five independent fields ($n = 3$). DT40 cells were simultaneously loaded with TOTO-3 and TMRE to assess plasma membrane integrity and $\Delta\psi_m$, respectively. (G and J) Functional mitochondria were not observed in either LPS (G) or BSO-sensitized WT DT40 (J) cells, but TMRE fluorescence could be restored by supplementation with 2.5 mM GSH. (H, I, K, and L) LPS and BSO had a trivial effect on either STIM1 KO (H and K) or Orai1 KO (I and L) cells. Error bars indicate mean ± SEM.

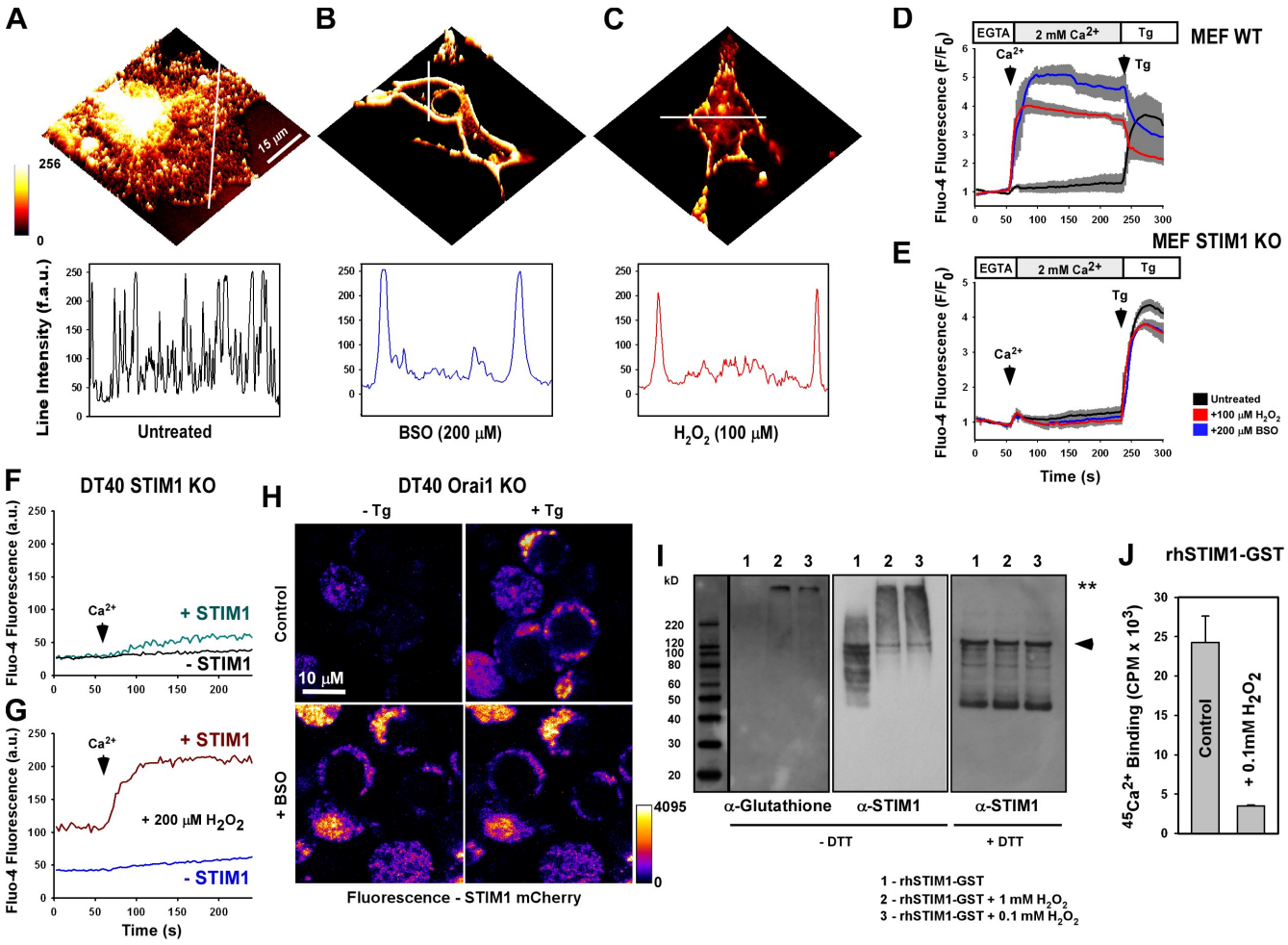

Figure 5. **Oxidative stress triggers store-independent STIM1 redistribution and CRAC activation via S-glutathionylation.** COS7 cells were transfected with WT STIM1 fused to the mCherry fluorescent construct. 36 h after transfection, STIM1 distribution was visualized via confocal microscopy. (A) STIM1 presents as an ER-resident protein in unstimulated cells, as demonstrated by fluorescence intensity through the perinuclear region. (B and C) STIM1 redistribution to discrete puncta near the plasma membrane is observed after either 200 μM BSO challenge for 24 h (B) or 20-min 100 μM H_2O_2 treatment (C). (A–C) Line scans indicate the distribution of STIM1-mCherry before and after the treatment. (D and E) Fluo-4–loaded WT MEF cells exposed to either BSO or H_2O_2 exhibited capacitive calcium entry without ER calcium store depletion by 2 μM Tg (D) that was not observed in STIM1 KO MEFs (E). Traces represent the mean fluorescence of all cells in the microscopic field. Values representing three independent experiments are displayed as a gray bar surrounding each trace. (F and G) Addition of 2 mM Ca^{2+} to the extracellular buffer in control (F) and after 20-min exposure to 200 μM H_2O_2 (G) in DT40 STIM1 KO cells. H_2O_2 challenge elicited store-independent Ca^{2+} entry upon addition of Ca^{2+}. STIM1-mCherry–negative cells were used as controls ($n = 3$). (H) Orai1 KO DT40 cells transfected with WT STIM1 mCherry before and 2.5 min after addition of 2 μM Tg. (I) Recombinant human STIM1 protein (rhSTIM1-GST) in buffer containing 10 mM GSH was incubated with 1 mM and 0.1 mM H_2O_2 for 30 min and resolved under nonreducing conditions. (left) Probed with α-glutathionylation antibody (**, S-glutathionylated STIM1). (middle) Stripped membrane reprobed with α-STIM1 antibody. (right) Probed with α-STIM1 antibody under reducing conditions. The arrowhead indicates native recombinant protein. Black line indicates that intervening lanes have been spliced out. (J) 200 μM $^{45}Ca^{2+}$-binding affinity (Luik et al., 2008; Stathopulos et al., 2008) of recombinant human STIM1 after incubation with 100 μM H_2O_2 for 30 min. $^{45}Ca^{2+}$ was assessed by liquid scintillation counting of duplicate protein filtrate samples and background corrected ($n = 5$). Error bars indicate mean ± SEM.

studied (Fig. 4 E). In stark contrast, STIM1 KO cells were protected from Ca^{2+}-mediated cell death throughout the duration of the experiment (Fig. 4 E). Supplementation of GSH reversed αIgM-induced cell death (1.5 μg/ml; 48 h) in DT40 cells challenged with either BSO or LPS (Fig. 4 F), indicating that the mechanism for both is mediated through GSH. Both STIM1 and Orai1 KO DT40 cells treated with either BSO or LPS were resistant to αIgM-induced cell death, as determined by nuclear incorporation of TOTO-3 (Fig. 4 F). Mechanistically, TOTO-3 staining was preceded by the loss of the mitochondrial membrane potential ($\Delta\Psi_m$) both in LPS (Fig. 4 G)- and BSO-treated (Fig. 4 J) cells, indicating a loss of mitochondrial function before cell death (Fig. 4, G and J, black dots). GSH supplementation restored $\Delta\Psi_m$ in WT DT40 cells (Fig. 4, G and J, red dots). Neither LPS nor BSO alone altered $\Delta\Psi_m$ in WT cells (unpublished data). Interestingly, $\Delta\Psi_m$ was unaltered in STIM1 and Orai1 KO cells (Fig. 4, H, I, K, and L). These findings clearly establish that sustained mitochondrial Ca^{2+} uptake, mitochondrial dysfunction, and cell death during oxidative stress are dependent on GSH bioavailability and CRAC-mediated Ca^{2+} entry.

Oxidative stress stimulates STIM1 puncta formation and store-independent calcium entry

Upon store depletion, STIM1 oligomerizes, redistributes, and binds to the plasma membrane–localized protein Orai1/CRACM1

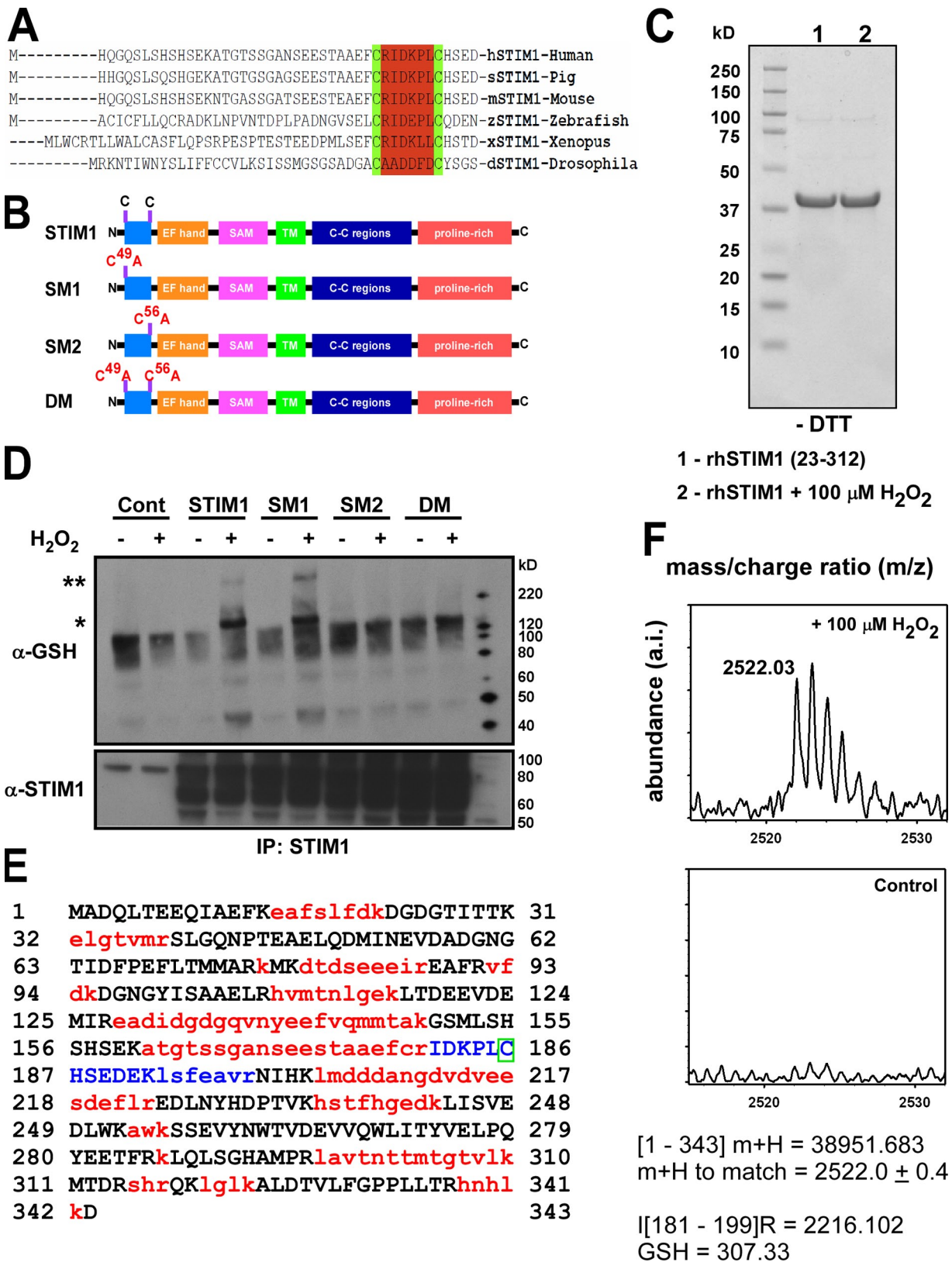

Figure 6. **Identification of cysteine 56 as the site for S-glutathionylation in response to oxidants.** (A) Sequence alignment of STIM1 demonstrates evolutionary conservation of cysteine residues at positions 49 and 56. (B) Schematic for STIM1 mutant constructs. (C) Coomassie staining of a truncated N-terminal STIM1 fragment (amino acids 23–213) exposed to 100 mM H_2O_2 for 30 min and run on a 4–12% Bis-Tris gel under nonreducing conditions (−DTT). No shift in protein mobility was detected, indicating that oxidant stress did not facilitate the formation of disulfide bonds in the STIM1 protein. (D) COS7 cell lysates from STIM1-transfected cells were incubated with 200 μM H_2O_2 for 30 min and immunoprecipitated (IP) with an α-STIM1 antibody. Immunoprecipitated STIM1 was resolved by electrophoresis under nonreducing conditions (−DTT) and probed for S-glutathionylation using a small peptide antibody against GSH. Nontreated samples were also resolved under reducing conditions (+DTT) and probed for STIM1 for input control. A truncated N-terminal

to form the CRAC channel and trigger Ca^{2+} entry and refilling of the ER stores (Prakriya et al., 2006). As our work demonstrates that oxidative stress enhances Ca^{2+} influx, we hypothesized that the STIM1 cellular distribution may be altered during oxidative stress. Because STIM1 is a dynamic protein, we chose to overexpress fluorescently tagged (mCherry) STIM1 in COS-7 cells to visualize its localization in live cells. In unstimulated COS-7 cells, STIM1 presents primarily as an ER-resident protein (Fig. 5 A). However, both 100 µM BSO challenge (Fig. 5 B) and H_2O_2 (20 min; Fig. 5 C) triggered redistribution from the ER to sites near the plasma membrane, demonstrating that oxidant stress promotes STIM1 oligomerization and may, perhaps, trigger CRAC activation. Addition of Ca^{2+} to the extracellular milieu evoked robust Ca^{2+} entry in BSO- and H_2O_2-treated, but not untreated, mouse embryonic fibroblasts (MEFs; Fig. 5 D). In contrast, Ca^{2+} entry was not observed in STIM1 KO MEFs, excluding the possibility that BSO or H_2O_2 may facilitate Ca^{2+} entry through other mechanisms other than the CRAC channel (Fig. 5 E). Although it is possible that oxidant stress may deplete ER Ca^{2+}, addition of the SERCA (sarco-ER Ca^{2+} ATPase) of Ca inhibitor thapsigargin (Tg) resulted in the passive depletion of ER Ca^{2+} and subsequent capacitive Ca^{2+} entry upon reintroduction of extracellular Ca^{2+} (unpublished data), indicating intact ER Ca^{2+} stores and normal CRAC channel function. Furthermore, DT40 cells under 100 µM H_2O_2 challenge (30 min) exhibited similar levels of ER Ca^{2+} as the control (unpublished data). Although STIM1 overexpression by itself did not induce constitutive Ca^{2+} entry (Fig. 5 F), short-term exposure to 200 µM H_2O_2 triggered capacitive Ca^{2+} entry without the need for ER store depletion by Tg (Fig. 5 G) in DT40 STIM1 KO cells overexpressing STIM1. In these experiments, DT40 cells were incubated with H_2O_2 for 20 min in Ca^{2+}-containing conditions and transferred to the experimental buffer lacking Ca^{2+}. Interestingly, because of this experimental methodology, we observed higher basal cytosolic Ca^{2+} levels in STIM1-positive cells versus STIM1-negative neighboring cells (Fig. 5 G), indicating the rapid activation of oxidant-triggered, STIM1-mediated Ca^{2+} entry. Nontransfected neighboring cells did not exhibit store-independent Ca^{2+} entry, further supporting that the H_2O_2 effect did not reflect oxidant-mediated ER Ca^{2+} depletion but, rather, required the expression of STIM1. Furthermore, BSO challenge in Orai1 KO cells did not result in CRAC activation (Fig. S4); however, the formation of STIM1 clusters remained unaffected (Fig. 5 H), revealing that STIM1, not Orai1, may be a target for cellular oxidants. Further investigation revealed that STIM1 puncta formation was dependent on the ER-luminal portion of the protein (Fig. S5).

A prominent molecular target of H_2O_2 is the reactive thiol group of the amino acid cysteine. Protein thiol groups react with H_2O_2 to yield sulfenic acid (R-SOH), which undergoes nucleophilic attack by RSH, resulting in disulfide formation (RSSR). Under oxidative conditions, GSSG can react with reactive thiol groups on proteins in this fashion in a process known as S-glutathionylation, which results in protein-specific functional changes. Under BSO-induced stress, S-glutathionylation is effectively an irreversible process because of the lack of free GSH needed to remove GSH via glutaredoxins. To test whether STIM1 is a target of S-glutathionylation, 0.3 µg recombinant human STIM1 was subjected to H_2O_2 in the presence of 10 mM GSH in a cell-free system. H_2O_2 challenge resulted in a strong S-glutathionylation signature, as detected by Western blotting (Fig. 5 I). Furthermore, S-glutathionylation was associated with a marked shift in molecular mass, implying that S-glutathionylation of STIM1 results in oligomer formation, a key step in CRAC activation. Addition of the reducing agent DTT normalized protein mobility in response to H_2O_2, indicating the reversibility of STIM1 S-glutathionylation. Mechanistically, H_2O_2-mediated S-glutathionylation decreases the Ca^{2+}-binding affinity of STIM1 (Fig. 5 J), thereby decoupling ER Ca^{2+} levels from CRAC activation.

Identification of cysteine 56 as the site for STIM1 S-glutathionylation

STIM1 is an evolutionarily conserved protein that is composed of a single transmembrane domain with a Ca^{2+}-binding domain (EF hand) and a sterile α-motif at the N terminus and a coiled-coil region and proline-rich C terminus (Baba et al., 2006). Analysis of the formation of active STIM1–Orai1 complexes revealed that CRAC formation is dependent on the STIM1 C terminus, which is activated in response to ER Ca^{2+} depletion (Park et al., 2009; Yuan et al., 2009). Although considerable heterogeneity exists between species, a defining feature of STIM1 is the presence of two highly conserved cysteine residues in the N-terminal region, which is located within the ER lumen near the EF hand (Fig. 6 A). Deletion of these residues along with the EF hand resulted in constitutive store-independent Ca^{2+} entry (Zhang et al., 2005). As cysteine residues are important targets for oxidants via either direct modification (e.g., intramolecular disulfide bonds or R-SOH formation) or S-glutathionylation, we therefore chose to investigate the role of these two conserved cysteine residues in STIM1-mediated Ca^{2+} entry (Fig. 6 B). Exposure of the STIM1 N-terminal region (amino acids 23–312), containing the EF hand and cysteine residues 49 and 56, to 100 µM H_2O_2 for 30 min did not alter protein mobility under nonreducing conditions (i.e., without DTT), suggesting that oxidant stress did not directly modify STIM1 (Fig. 6 C). Because STIM1 can be directly S-glutathionylated in the presence of oxidants (Fig. 5 I), we next sought to identify which reactive cysteine serves as molecular target of oxidants in intact cells. Although no S-glutathionylation signature was detected under normal

STIM1 fragment (amino acids 23–312) was subjected to tryptic digestion and assessed for S-glutathionylation at cysteine 56 by mass spectrometry. *, S-glutathionylation of STIM1; **, higher molecular mass STIM1 after H_2O_2 treatment. (E) Sequence of recombinant STIM1 fragment. Red indicates sequences not detected by MALDI time of flight. Blue indicates that the sequence contains cysteine 56. The green box indicates that the presence of GSH in this fragment can only be associated with the cysteine residue at position 56. (F) 30-min exposure of recombinant STIM1 protein to 100 µM H_2O_2 resulted in the formation of a mass spectra at a calculated mass of 2,522.0 ± 0.4 kD that was absent in the nontreated sample, corresponding to an increase of 306 to the predicted mass of the blue peptide fragment in D (2,216.102 kD). The molecular mass of reduced GSH is 307 D.

conditions, significant S-glutathionylation in both STIM1 and the SM1 mutant, but not the SM2 mutant, were observed after H_2O_2 challenge (Fig. 6 D), revealing the cysteine at position 56 as exquisitely sensitive to oxidant stress. As in our cell-free conditions, S-glutathionylation also resulted in the formation of a large molecular mass protein under nonreducing conditions (Fig. 6 D, **). Importantly, the mechanism is reversible, as resolving these proteins under reducing conditions revealed no S-glutathionylation in any of the STIM1 mutants (unpublished data). To conclusively demonstrate the identity of the glutathionylated residues on STIM1, the recombinant N-terminal region (amino acids 23–312) of STIM1 was exposed to 100 µM H_2O_2 in the presence of 10 mM GSH. Tryptic digestion resulted in the separation of the cysteine residues at positions 49 and 56 into two distinct peptide fragments, with position 56 within the fragment containing amino acids 181–199 and a mass of 2,216.102 kD (Fig. 6 E, blue). In the H_2O_2-treated, but not the control sample, a mass spectra was found at 2,522.0 ± 0.4 kD (Fig. 6 F). This corresponds to the predicted fragment mass of 2,216.102 + 306 kD, which is the deprotonated molecular mass of GSH. Because GSH can only react with free thiol groups, the presence of GSH in this fragment can only be associated with the cysteine residue at position 56 (Fig. 6 E, green box). Together with protein mobility and immunoblotting, the detection of GSH clearly identifies that the two cysteine residues in the N-terminal region of STIM1 are not directly modified by oxidants, but rather, cysteine 56 is a site for S-glutathionylation in the presence of oxidants.

Modification of STIM1 at cysteine 56 evokes constitutive CRAC activity

A fundamental question is whether cysteine 56 is crucial for CRAC channel activation. To test this, Ca^{2+} entry was measured in STIM1 KO DT40 cells after the reexpression of mCherry-tagged WT, SM2, and double-mutant (DM) STIM1 variants. Surprisingly, similar to BSO and H_2O_2 treatment, expression of STIM1 mutants (SM2 and DM) in STIM1 KO DT40 cells resulted in constitutive Ca^{2+} entry, as detected by confocal microscopy (Fig. 7, A and B). Reconstitution of WT STIM1 in STIM1 KO DT40 cells also rescued BSO-induced constitutive Ca^{2+} entry (Fig. 7, A and B), whereas nontransfected neighboring cells did not exhibit an increase in Ca^{2+} fluorescence (unpublished data). In addition, introduction of the SM2 mutant increased ROS production in DT40 STIM1 KO cells to similar levels as BSO challenge (unpublished data). Moreover, in HEK293T cells, SM2 or DM mutation resulted in a substantial redistribution of STIM1 toward the plasma membrane, where it colocalized with Orai1 (Fig. 7 C). Functionally, overexpression of SM2 resulted in the formation of puncta (Fig. 7 C) and a constitutive CRAC current that was independent of the ER Ca^{2+} stores (Fig. 7, D–F).

Discussion

Molecular identification of STIM1 as the ER Ca^{2+} sensor in CRAC activation has greatly aided our understanding of Ca^{2+} signaling. However, a key question regarding how STIM1 is controlled remains unanswered; namely, what physiological cues can modulate STIM1-mediated Ca^{2+} entry. Oxidative stress has long been implicated in Ca^{2+} dysregulation. In particular, lymphocytes respond to oxidants by an increase in basal Ca^{2+} levels (Howe et al., 2004). Although it is possible that oxidants may affect ER Ca^{2+} release or inhibit reuptake by SERCA pumps, the present findings suggest that oxidants directly decrease STIM1 Ca^{2+}-binding affinity via S-glutathionylation at cysteine 56, facilitating constitutive Ca^{2+} entry and elevating basal cytosolic Ca^{2+} levels. This is supported by our findings that STIM1 KO DT40 cells are immune to LPS- and BSO-induced oxidative stress and that reintroduction of STIM1 into STIM1 KO DT40 lymphocyte cells markedly elevated basal cytosolic Ca^{2+} levels when exposed to oxidant stress compared with nontransfected neighboring cells (Fig. 5 G). Furthermore, genetic removal of either STIM1 (Fig. 5 E) or Orai1 (Fig. S4) eliminated constitutive CRAC activation in response to oxidant challenge. Therefore, these data are the first to definitively link Ca^{2+} regulation and cellular redox status and establish STIM1 as an important sensor for oxidative stress.

LPS is a common inflammatory signal inducer that initiates ROS production through Toll-like receptor 4 (Park et al., 2004), leading to extensive proliferation and differentiation in leukocytes (Coutinho et al., 1974). In contrast, B cell receptor antigen cross-linking can trigger several outcomes, including activation, proliferation, or death, depending on the stage of B cell development (Khan, 2009). However, costimulation by both LPS and antigens acts synergistically to sensitize B cells (Minguet et al., 2008), possibly allowing the immune system to focus B cell maturation only on antigen-presenting B cells (Ruprecht and Lanzavecchia, 2006). After activation, unregulated lymphocyte proliferation would exacerbate the immune response and could lead to the development of autoimmune diseases such as rheumatoid arthritis (Busconi et al., 2007). Based on our findings, it is possible that chronic mitochondrial ROS generation serves to limit lymphocyte activation through a gradual reduction in mitochondrial energy production, thus acting as a stop signal that limits the immune response. Costimulation of inflammatory molecules that generate ROS and mobilize Ca^{2+} exist in several different tissues aside from lymphocytes, including LPS and CD14 in dendritic cells (Zanoni et al., 2009) and TNF and leukotriene B4 in endothelial cells (Qiu et al., 2006). Therefore, we postulate that enhancement of CRAC by S-glutathionylation activation is the mechanism whereby ROS and Ca^{2+} synergistically modulate inflammation. Because elevated basal Ca^{2+} was also noted in other cell types, including HEK293, COS-7 (unpublished data), and the ubiquitous expression of STIM1, oxidant-regulated, STIM1-mediated Ca^{2+} entry may be an important physiological process in many tissues. S-glutathionylation of STIM1 correlated with an approximately threefold decrease in GSH from normal cellular levels (Fig. 3 H).

The defining step in CRAC activation is STIM1 oligomerization that follows Ca^{2+} dissociation from the EF hand region (Smyth et al., 2008). Structurally, it is believed that Ca^{2+} dissociation disrupts interactions between the EF hand and sterile α-motif domains and results in STIM1 destabilization and partial unfolding, which facilitates oligomerization of STIM1 and

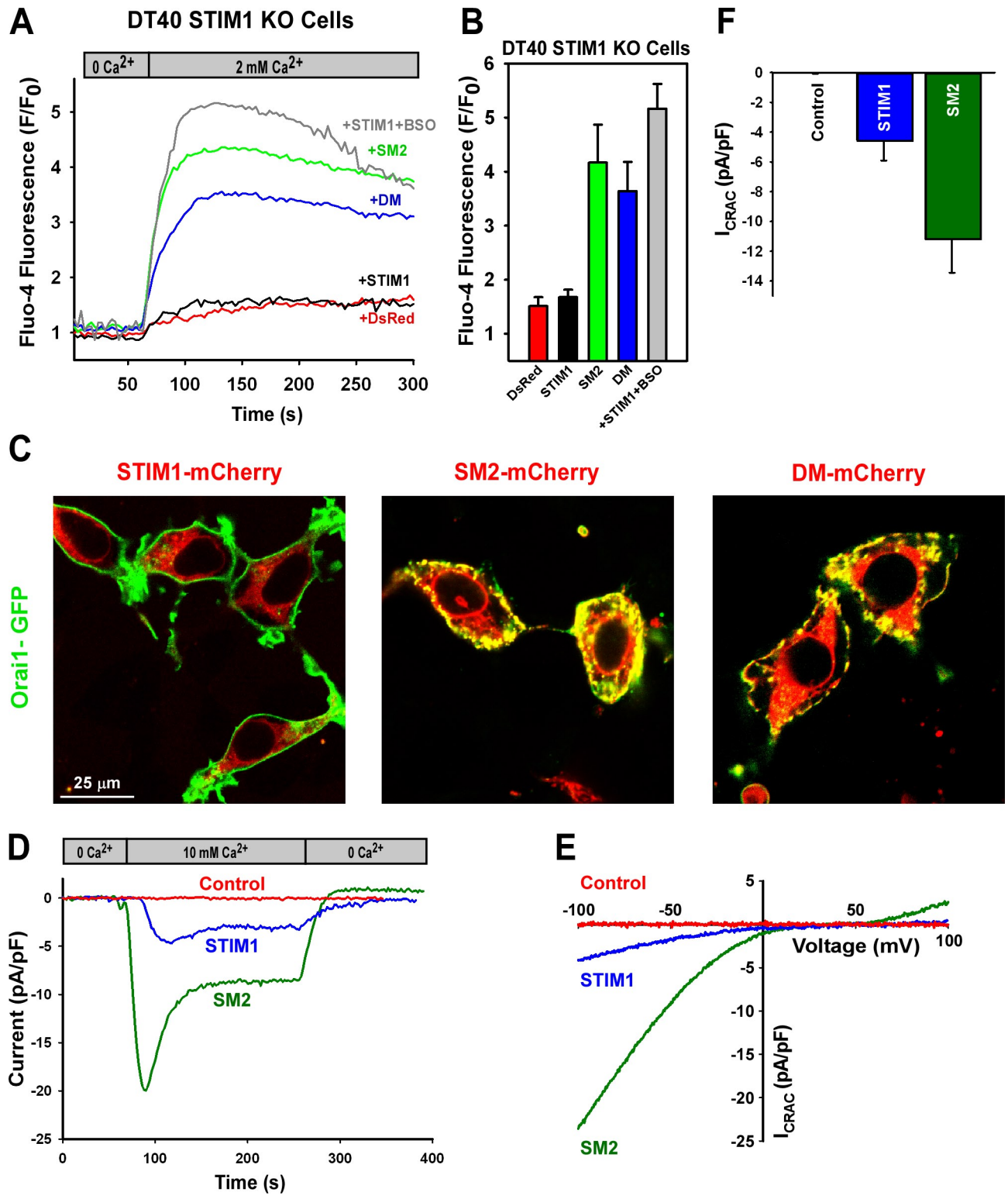

Figure 7. **Constitutive activation of STIM1 by point mutation of cysteine 56.** (A) DT40 STIM1 KO cells transfected with STIM1-mCherry mutant constructs were loaded with Fluo-4 and fluorescence changes recorded after addition of Ca^{2+} to the extracellular milieu. SM2 and DM constructs demonstrated store-independent Ca^{2+} entry versus WT STIM1 and DsRed (control) constructs. WT STIM1 pretreated with BSO exhibited constitutive Ca^{2+} entry. Traces represent mean fluorescence values. (B) Mean fluorescence intensity within 90 s of Ca^{2+} addition in at least three independent experiments. (C) HEK293T cells transfected with both STIM1-mCherry and Orai1-GFP. SM2 and DM constructs demonstrate STIM1 redistribution and Orai1 colocalization. Conventional whole cell recordings were performed in HEK293 CFP-Orai1 stable cells transfected with control, WT, or SM2 STIM1-mCherry constructs. (D) Typical time course of CRAC current after addition and removal of 10 mM calcium in HEK293 Orai1-CFP cells with cytosolic Ca^{2+} levels clamped at rest. (E) Representative current–voltage relationship of the CRAC current at maximal activation in 10 mM Ca^{2+}. (F) Quantitation of peak CRAC current shown in E at −100 mV (n = 8 cells). Error bars indicate mean ± SEM.

CRAC activation (Stathopulos et al., 2008). Because of their proximity to the EF hand, the highly conserved cysteine residues at positions 49 and 56 were considered potential target sites of oxidants via intra- or intermolecular disulfide bonds or through S-glutathionylation. Initially, we hypothesized that replacing the cysteine residues with the nonreactive amino acid alanine would ablate oxidant-induced constitutive Ca^{2+} entry. Surprisingly, cells transfected with mutant STIM1 constructs displayed dramatic redistribution of STIM1 into discrete puncta near the plasma membrane and higher basal Ca^{2+} levels and CRAC activation, which is indicative of STIM1 oligomerization. Although unexpected, this finding is consistent with a previous study in which point mutation of single amino acids within the EF hand led to CRAC activation (Zhang et al., 2005). Likely, by virtue of its close proximity to the EF hand region of STIM1 (10 amino acids), either mutation or S-glutathionylation of cysteine 56 alters protein confirmation enough to decrease Ca^{2+}-binding affinity and activate the protein. Of these mutants, we identified that WT STIM1 and the SM1 mutation ($C^{49}A$) mutants formed large molecular mass structures in the presence of H_2O_2 under nonreducing conditions (Fig. 6 D, **). Furthermore, this STIM1 S-glutathionylation appears to be a nonenzymatic process, as GSH was detected both by immunoblotting (Fig. 5 I) and mass spectrometry (Fig. 6 F) in a cell-free system. Reducing the samples with DTT removed GSH from the cysteine at position 56 (unpublished data) and disrupted the formation of these large molecular mass oligomers (Fig. 5 I), effectively demonstrating the reversibility of this mechanism. Functionally, STIM1 S-glutathionylation serves to reduce the Ca^{2+}-binding affinity of the EF hand region (Fig. 5 J), effectively activating STIM1 independent of ER calcium levels. A recent study demonstrated that STIM1 oligomerization is the switch that links ER store depletion and CRAC activation (Luik et al., 2008). However, the study used an artificial system to oligomerize STIM1 independent of ER Ca^{2+} levels. Our experiments are the first to demonstrate reversible STIM1 oligomerization independent of ER Ca^{2+} stores using a physiological model of chronic autocrine-derived oxidant stress. In contrast, acute challenge with H_2O_2 (paracrine) triggered inactivation of Orai1-dependent CRAC activity (Bogeski et al., 2010). Although contradictory to this finding, we postulate that our model of chronic autocrine oxidant production serves a different cellular response than that of an acute oxidant challenge.

In contrast to transient Ca^{2+} elevations, which restrict the actions of Ca^{2+} to specific, high affinity targets, chronic elevations in cytosolic Ca^{2+} extend the duration for Ca^{2+} binding (Boulware and Marchant, 2008). Thus, sustained Ca^{2+} elevations can influence additional cellular processes such as transcription (Dolmetsch et al., 1997) and enzyme activation (Leslie, 1997). Our data suggests that sustained Ca^{2+} elevations also govern mitochondrial Ca^{2+} handling. Elevated cytosolic Ca^{2+} triggers mitochondrial Ca^{2+} uptake by the Ca^{2+} uniporter (Kirichok et al., 2004), which is then inactivated by sustained Ca^{2+} levels (Parekh, 2008). Both LPS- and BSO-induced oxidative stress elicited mitochondrial Ca^{2+} uptake in a step-wise manner (Fig. 1 A; Fig. 2, F and M; Fig. 4 C; Fig. S1; and Fig. S3). The magnitude of each of these step-wise increases was similar to physiological Ca^{2+} transients seen in nonstressed mitochondria (Fig. 2, A and L; Fig. 4 A; and Fig. S1), which is indicative of intact uniporter function. These results suggest that chronic STIM1-mediated elevation in cytosolic Ca^{2+} is likely sufficient to sensitize the mitochondria either by inhibiting the inactivation phase of the uniporter or altering mitochondrial Ca^{2+} extrusion. In addition to STIM1, S-glutathionylation of mitochondrial proteins can also occur and has been linked to both cell death and survival. Reversible glutathionylation of complex I increases mitochondrial superoxide formation that leads to oxidative damage and cell death (Taylor et al., 2003). Furthermore, deglutathionylation of complex II decreases mitochondrial electron transfer activity during myocardial ischemia and reperfusion injury (Chen et al., 2007). In contrast, S-glutathionylation of adenine nucleotide translocase via carbon monoxide prevents loss of mitochondrial membrane permeabilization and apoptosis (Queiroga et al., 2010). In this study, we demonstrate that the S-glutathionylation of the ER-resident protein STIM1 affects the mitochondrial homeostasis via CRAC activation and an elevation in cytosolic Ca^{2+}.

In conclusion, these findings demonstrate a relationship between oxidative stress and STIM1-mediated Ca^{2+} entry. By reversibly targeting the highly conserved cysteine 56 residue near the EF hand, oxidant-induced S-glutathionylation decreases Ca^{2+} binding, triggering STIM1 oligomerization and CRAC activation independent of ER Ca^{2+} stores. Constitutive activation of the CRAC channel facilitates an increase in Ca^{2+} levels both at rest and after cellular activation (i.e., increases in diastolic Ca^{2+}). This sustained Ca^{2+} increase enhances mitochondrial Ca^{2+} loading and influences mitochondrial function, which over time can trigger cell death. Because of the widespread tissue expression of STIM1, this mechanism is likely to be involved in many different cell types and may play an important role in both physiological and pathological signaling by ROS.

Materials and methods

Cell culture

WT (DT40 WT), STIM1 KO (DT40 STIM1 KO), and Orai KO B cell lines were cultured in RPMI 1640 supplemented with 10% FCS, 1% chicken serum, and antibiotics. HEK293T, COS7, and MEF (WT and STIM1 KO) cell lines were cultured in DME supplemented with 10% FCS and antibiotics. To induce oxidative stress, LPS (Sigma-Aldrich) or BSO (Sigma-Aldrich) was added at the indicated concentration 5 and 24 h before experimentation, respectively. BHA (Sigma-Aldrich) was added to cells 1 h before LPS challenge.

Measurement of cytosolic and mitochondrial Ca^{2+} concentration ($[Ca^{2+}]_c$ and $[Ca^{2+}]_m$)

DT40 cells were affixed to Cell-Tak–coated (BD) 25-mm glass coverslips and loaded with 5 µM Fluo-4/AM in extracellular medium (ECM) as described previously (Madesh et al., 2005). For simultaneous measurement of $[Ca^{2+}]_c$ and mitochondrial Ca^{2+} uptake, cells were loaded with 2 µM rhod-2/AM (Invitrogen) and 5 µM Fluo-4/AM in ECM followed by an additional 10-min incubation in a dye-free medium. Coverslips were placed in a chamber and mounted in an open perfusion microincubator (PDMI-2; Harvard Apparatus) and maintained at 37°C on an inverted microscope (TE300 [Nikon] and Axio Observer [Carl Zeiss, Inc.]). 5 µg/ml mouse anti–chicken IgM (SouthernBiotech) was added after 1 min of baseline recording, and images were recorded every 3 s using a confocal imaging system (Radiance 2000; Bio-Rad Laboratories) or a laser-scanning confocal system (510 Meta; Carl Zeiss, Inc.) equipped with an Argon ion laser source at 488- and 568-nm excitation using a 60× oil objective. Images were

acquired using either Lasersharp or ZEN 2008 software (Carl Zeiss, Inc). Images were analyzed and quantitated using ImageJ (National Institutes of Health) and a custom-made software (Spectralyzer). To assess Ca^{2+} entry, Ca^{2+}-free ECM was used in conjunction with 0.5 mM EGTA. 2 mM Ca^{2+} was added as indicated.

GSH measurement

GSH concentration was assessed via the reaction of GSH with Ellman's reagent using a spectrophotometer according to the manufacturer's protocol (Cayman Chemical). GSH was measured in intact cells using the fluorescent compound MCB (Invitrogen). In brief, 10 µM MCB was added directly to DT40 cells in complete medium and allowed to incubate at 40°C for 20 min. MCB will enter cells and bind to GSH to form the fluorescent adduct GSH-MCB. MCB will not react with oxidized GSSG. After loading, cells were washed, resuspended in HBSS, and fluorescence recorded using a confocal system (510 Meta) with excitation at 488 nm.

Detection of ROS

WT and STIM1 KO DT40 cells were challenged with 200 µM BSO. 24 h after BSO addition, cells were stained with 10 µM HE or 5 µM 5-(and-6)-chloromethyl-2′7′-dichlorodihydrofluorescein diacetate acetyl ester (CM-H_2DCF-DA or DCF) to detect superoxide anion and H_2O_2, respectively. Cells were washed, spun, and placed on the stage of a confocal imaging system (510 Meta). Excitation was 561 nm and 488 nm for HE and DCF, respectively. Images were analyzed using ImageJ software. For a positive control, BSO-treated DT40 STIM1 KO cells were incubated with 1 mM H_2O_2 for 30 min during DCF staining.

STIM1 S-glutathionylation

Recombinant human GST-tagged STIM1 was purchased from Abnova. 0.3 mg protein (in buffer containing 10 mM GSH) was incubated with either 1.0 or 0.1 mM H_2O_2 for 30 min at 23°C. Samples were resolved on a 4–12% Bis-Tris gel in the absence of reducing agents and probed with α-GSH antibody (1:1,000; Virogen). The membrane was then stripped and probed with α-STIM1 (1:500; BD).

$^{45}Ca^{2+}$-binding experiments

Calcium binding to STIM1 was assessed as the protein-bound radioactivity retained after ultrafiltration procedure as described previously with minor modification (Ames et al., 2000). In brief, full-length GST-tagged STIM1 recombinant protein (Abnova) was subjected to the S-glutathionylation reaction as described in the previous paragraph. Both control and 0.1 mM H_2O_2–treated WT recombinant STIM1 (600 ng/sample) protein was incubated with 0.2 mM $^{45}CaCl_2$ in phosphate-buffered saline, pH 7.4, for 30 min at room temperature. After washing twice, the radioactivity in the protein-containing solution was determined by liquid scintillation counting.

Mitochondrial oxygen consumption

Oxygen consumption was measured using MitoCell (MT200; Strathkelvin Instruments). In brief, 10^7 DT40 cells were washed in ECM, pelleted, resuspended, permeabilized in 110 µl intracellular medium containing 40 µg/ml digitonin, and placed into the MT200 chamber at 40°C under constant stirring. The oxygen electrode was calibrated using air-saturated ddH_2O and the oxygen chelator Na_2SO_3 for 21% and 0% dissolved oxygen, respectively. After 30-s equilibration, the following additions were added in the following order: 5 mM malate/pyruvate, 100 nM rotenone, 5 mM succinate, 50 nM antimycin A, 5 mM ascorbate/0.25 mM TMPD (tetramethyl-*p*-phenylenediamine), and 1 µM CCCP. Representative traces are displayed and are indicative of three independent experiments.

Cell viability

Untreated and 200 µM BSO–treated cells were activated with 1.5 µg/ml αIgM every 24 h, and cell viability was determined via nuclear TOTO-3 (Invitrogen) incorporation. In brief, cells were pelleted, stained with TOTO-3 (1:1,400), and imaged at 633/660-nm excitation/emission using a confocal imaging system (510 Meta). TOTO-3 is normally membrane impermeable and only becomes incorporated into the nucleus when the plasma membrane is compromised. In some experiments, untreated cells and those treated with either LPS or BSO were simultaneously loaded with TOTO-3 and the mitochondrial membrane potential indicator tetramethylrhodamine, ethyl ester (TMRE) to determine cell viability and mitochondrial function, respectively. Cells were challenged with BSO as above and 1 µg/ml LPS every 24 h. Samples were loaded with TOTO-3 and 100 nM TMRE for 15 min and imaged at 633/660-nm and 561/590-nm excitation/emission, respectively. Images were collected from five independent microscopic fields for three independent experiments, and simultaneous fluorescence was measured using ImageJ. Values indicate mean ± SEM (n = 3). Simultaneous fluorescence scatter plots for at least 600 data points are represented for both TOTO-3 and TMRE.

STIM1-mCherry mutation and cell transformation

Substitution of alanine for cysteine at positions 49 and 56 in STIM1-mCherry constructs was performed using a site-directed mutagenesis kit (Quikchange; QIAGEN). COS7 and HEK293T cell lines were transfected using TransIT reagent according to manufacturer's protocol (Mirus Bio LLC). DT40 cells were transfected via electroporation of 0.5×10^6 cells in 0.5 ml RPMI using a gene pulsar apparatus (340 V and 950 microfarads; Bio-Rad Laboratories). STIM1 puncta were assessed using the WT STIM1-mCherry construct in Orai1 KO DT40 cells. In brief, cells transfected via electroporation were fixed on Cell-Tak–coated coverslips and imaged at 561 nm both before and after Tg addition in the presence or absence of BSO. YFP-STIM1ΔK (1–666), GFP-SOAR-LQ347/348AA, and mCherry-Orai1 were N-terminally labeled and were provided by S. Muallem (University of Texas Southwestern Medical Center, Dallas, TX).

Mass spectrometry

Recombinant N-terminal portion of the STIM1 protein tagged with 0.3 µg calmodulin (Novus Biologicals) was incubated with 100 µM H_2O_2 in the presence of 10 mM GSH for 30 min as previously described (Aracena-Parks et al., 2006). Control conditions were incubated with 10 mM GSH without H_2O_2. Proteins were precipitated in acetone from the buffer solution. Two enzymes were used for the protein digestion: sequencing grade modified trypsin (Promega) and endoproteinase Asp-N (Roche) at 35°C overnight. For matrix-assisted laser desorption/ionization (MALDI) time of flight peptide mass fingerprinting, 0.3 µl digested peptides and 0.3 µl matrix (CHCA; Fluka) were spotted onto a MALDI target plate and allowed to dry. Mass spectra were acquired with a mass spectrometer (Reflex IV; Bruker Daltonics) between 500 and 5,000 m/z in reflectron mode and peptide peaks internally calibrated using trypsin autolysis peaks.

Immunoblotting

Protein lysates were prepared from COS7 cells transfected with STIM1 WT and mutant plasmids 36 h after transfection. Samples were immunoprecipitated with an α-STIM1 antibody and divided into two aliquots: one prepared with loading buffers lacking DTT (nonreducing conditions), and one prepared in DTT-containing loading buffers. Proteins were resolved on a 4–12% Bis-Tris gel (Invitrogen) and blotted with α-STIM1 (BD) and α-GSH (Virogen) antibodies for reducing and nonreducing conditions, respectively. After initial blotting, the α-STIM1 was stripped and reprobed with α-GSH to determine the S-glutathionylation reversibility. Plasma membrane Ca^{2+} ATPase levels in DT40 cells were assessed by immunoblotting. Anti-PMCA1/4 was purchased from Santa Cruz Biotechnology, Inc. (PMCA1/4).

Electrophysiology

In brief, linear voltage ramps of 50-ms duration spanning the voltage range of −100 to 100 mV were delivered from a holding potential of 0 mV at a rate of 0.5 Hz. The currents were filtered at 6 kHz and sampled at 10–50-µs intervals. We used automatic capacitive and series resistance compensation of the amplifier (EPC-10; HEKA). The intracellular solution contained 145 mM CsGlu, 10 mM Hepes, 10 mM EGTA, 8 mM NaCl, 6 mM $MgCl_2$, 2 mM Mg-ATP (total 8 mM Mg^{2+}), and 3 mM $CaCl_2$, pH 7.2. 8 mM Mg^{2+} and ATP were used to inhibit TRPM7. According to WEBMAXCLITE (http://www.stanford.edu/~cpatton/webmaxc/webmaxclite115.htm), the free Ca^{2+} concentration was 100 nM. The extracellular solutions contained 145 mM NaCl, 10 mM $CaCl_2$, 10 mM CsCl, 2 mM $MgCl_2$, 2.8 mM KCl, 10 mM Hepes, and 10 mM glucose, pH 7.4. For Ca^{2+}-free solution, 10 mM $CaCl_2$ was replaced by 10 mM $MgCl_2$.

Online supplemental material

Fig. S1 shows the dose-dependent alterations in αIgM-induced calcium mobilization and mitochondrial calcium uptake in response to increasing concentrations of BSO. Fig. S2 demonstrates that Orai1 is requisite for the phenotypic alteration in calcium mobilization observed during oxidative stress. Fig. S3 shows the restoration of transient mitochondrial calcium uptake by elimination of capacitative calcium entry. Fig. S4 shows that Orai1 KO cells do not exhibit calcium entry in response to BSO. Fig. S5 illustrates that puncta formation under oxidant stress is dependent on the STIM1 N-terminal region. Online supplemental material is available at http://www.jcb.org/cgi/content/full/jcb.201004152/DC1.

We would like to thank Drs. Anjana Rao, Richard Lewis, Tamas Balla, and Shmuel Muallem for the STIM1 KO MEFs, STIM1-mCherry, Orai1-GFP, and STIM1ΔK (1–666) and STIM1 SOAR-LQ347/348AA plasmids, respectively. We thank the Fox Chase Cancer Center Proteomics facility for mass spectrometry studies. We would also like to thank Dr. Sheldon Feinstein, Mark Bollman, Pranavi Vemuri, and Roma Rajput for their experimental assistance.

This work was supported by the National Institutes of Health (grants HL086699, HL086699-01A2S1, and 1S10RR027327-01) and the American Heart Aassociation (Scientist Development grant to M. Madesh). B.J. Hawkins was supported by the National Institutes of Health (grant K99HL094536) and a postdoctoral fellowship from the Pulmonary Hypertension Association. S.K. Joseph is supported by the National Institutes of Health (grant DK34804).

Submitted: 18 February 2010
Accepted: 8 July 2010

References

Ames, J.B., K.B. Hendricks, T. Strahl, I.G. Huttner, N. Hamasaki, and J. Thorner. 2000. Structure and calcium-binding properties of Frq1, a novel calcium sensor in the yeast *Saccharomyces cerevisiae*. *Biochemistry.* 39:12149–12161. doi:10.1021/bi0012890

Anathy, V., S.W. Aesif, A.S. Guala, M. Havermans, N.L. Reynaert, Y.S. Ho, R.C. Budd, and Y.M. Janssen-Heininger. 2009. Redox amplification of apoptosis by caspase-dependent cleavage of glutaredoxin 1 and S-glutathionylation of Fas. *J. Cell Biol.* 184:241–252. doi:10.1083/jcb.200807019

Aracena-Parks, P., S.A. Goonasekera, C.P. Gilman, R.T. Dirksen, C. Hidalgo, and S.L. Hamilton. 2006. Identification of cysteines involved in S-nitrosylation, S-glutathionylation, and oxidation to disulfides in ryanodine receptor type 1. *J. Biol. Chem.* 281:40354–40368. doi:10.1074/jbc.M600876200

Armstrong, J.S., and D.P. Jones. 2002. Glutathione depletion enforces the mitochondrial permeability transition and causes cell death in Bcl-2 overexpressing HL60 cells. *FASEB J.* 16:1263–1265.

Arrick, B.A., O.W. Griffith, and A. Cerami. 1981. Inhibition of glutathione synthesis as a chemotherapeutic strategy for trypanosomiasis. *J. Exp. Med.* 153:720–725. doi:10.1084/jem.153.3.720

Asehnoune, K., D. Strassheim, S. Mitra, J.Y. Kim, and E. Abraham. 2004. Involvement of reactive oxygen species in Toll-like receptor 4-dependent activation of NF-kappa B. *J. Immunol.* 172:2522–2529.

Baba, Y., K. Hayashi, Y. Fujii, A. Mizushima, H. Watarai, M. Wakamori, T. Numaga, Y. Mori, M. Iino, M. Hikida, and T. Kurosaki. 2006. Coupling of STIM1 to store-operated Ca2+ entry through its constitutive and inducible movement in the endoplasmic reticulum. *Proc. Natl. Acad. Sci. USA.* 103:16704–16709. doi:10.1073/pnas.0608358103

Berridge, M.J., M.D. Bootman, and H.L. Roderick. 2003. Calcium signalling: dynamics, homeostasis and remodelling. *Nat. Rev. Mol. Cell Biol.* 4:517–529. doi:10.1038/nrm1155

Bogeski, I., C. Kummerow, D. Al-Ansary, E.C. Schwarz, R. Koehler, D. Kozai, N. Takahashi, C. Peinelt, D. Griesemer, M. Bozem, et al. 2010. Differential redox regulation of ORAI ion channels: a mechanism to tune cellular calcium signaling. *Sci. Signal.* 3:ra24. doi:10.1126/scisignal.2000672

Bootman, M.D., C.W. Taylor, and M.J. Berridge. 1992. The thiol reagent, thimerosal, evokes Ca2+ spikes in HeLa cells by sensitizing the inositol 1,4,5-trisphosphate receptor. *J. Biol. Chem.* 267:25113–25119.

Boulware, M.J., and J.S. Marchant. 2008. Timing in cellular Ca2+ signaling. *Curr. Biol.* 18:R769–R776. doi:10.1016/j.cub.2008.07.018

Busconi, L., J.W. Bauer, J.R. Tumang, A. Laws, K. Perkins-Mesires, A.S. Tabor, C. Lau, R.B. Corley, T.L. Rothstein, F.E. Lund, et al. 2007. Functional outcome of B cell activation by chromatin immune complex engagement of the B cell receptor and TLR9. *J. Immunol.* 179:7397–7405.

Chen, Y.R., C.L. Chen, D.R. Pfeiffer, and J.L. Zweier. 2007. Mitochondrial complex II in the post-ischemic heart: oxidative injury and the role of protein S-glutathionylation. *J. Biol. Chem.* 282:32640–32654. doi:10.1074/jbc.M702294200

Coutinho, A., E. Gronowicz, W.W. Bullock, and G. Möller. 1974. Mechanism of thymus-independent immunocyte triggering. Mitogenic activation of B cells results in specific immune responses. *J. Exp. Med.* 139:74–92. doi:10.1084/jem.139.1.74

Crompton, M. 1999. The mitochondrial permeability transition pore and its role in cell death. *Biochem. J.* 341:233–249. doi:10.1042/0264-6021:3410233

Csordás, G., C. Renken, P. Várnai, L. Walter, D. Weaver, K.F. Buttle, T. Balla, C.A. Mannella, and G. Hajnóczky. 2006. Structural and functional features and significance of the physical linkage between ER and mitochondria. *J. Cell Biol.* 174:915–921. doi:10.1083/jcb.200604016

Dalle-Donne, I., R. Rossi, G. Colombo, D. Giustarini, and A. Milzani. 2009. Protein S-glutathionylation: a regulatory device from bacteria to humans. *Trends Biochem. Sci.* 34:85–96. doi:10.1016/j.tibs.2008.11.002

Deng, X., Y. Wang, Y. Zhou, J. Soboloff, and D.L. Gill. 2009. STIM and Orai: dynamic intermembrane coupling to control cellular calcium signals. *J. Biol. Chem.* 284:22501–22505. doi:10.1074/jbc.R109.018655

Diehn, M., R.W. Cho, N.A. Lobo, T. Kalisky, M.J. Dorie, A.N. Kulp, D. Qian, J.S. Lam, L.E. Ailles, M. Wong, et al. 2009. Association of reactive oxygen species levels and radioresistance in cancer stem cells. *Nature.* 458:780–783. doi:10.1038/nature07733

Dolmetsch, R.E., R.S. Lewis, C.C. Goodnow, and J.I. Healy. 1997. Differential activation of transcription factors induced by Ca2+ response amplitude and duration. *Nature.* 386:855–858. doi:10.1038/386855a0

Duchen, M.R. 2000. Mitochondria and calcium: from cell signalling to cell death. *J. Physiol.* 529:57–68. doi:10.1111/j.1469-7793.2000.00057.x

Feske, S. 2007. Calcium signalling in lymphocyte activation and disease. *Nat. Rev. Immunol.* 7:690–702. doi:10.1038/nri2152

Filippin, L., P.J. Magalhães, G. Di Benedetto, M. Colella, and T. Pozzan. 2003. Stable interactions between mitochondria and endoplasmic reticulum allow rapid accumulation of calcium in a subpopulation of mitochondria. *J. Biol. Chem.* 278:39224–39234. doi:10.1074/jbc.M302301200

Gilabert, J.A., D. Bakowski, and A.B. Parekh. 2001. Energized mitochondria increase the dynamic range over which inositol 1,4,5-trisphosphate activates store-operated calcium influx. *EMBO J.* 20:2672–2679. doi:10.1093/emboj/20.11.2672

Howe, C.J., M.M. Lahair, J.A. McCubrey, and R.A. Franklin. 2004. Redox regulation of the calcium/calmodulin-dependent protein kinases. *J. Biol. Chem.* 279:44573–44581. doi:10.1074/jbc.M404175200

Huddleston, A.T., W. Tang, H. Takeshima, S.L. Hamilton, and E. Klann. 2008. Superoxide-induced potentiation in the hippocampus requires activation of ryanodine receptor type 3 and ERK. *J. Neurophysiol.* 99:1565–1571. doi:10.1152/jn.00659.2007

Ihara, Y., K. Kageyama, and T. Kondo. 2005. Overexpression of calreticulin sensitizes SERCA2a to oxidative stress. *Biochem. Biophys. Res. Commun.* 329:1343–1349. doi:10.1016/j.bbrc.2005.02.112

Kaplan, P., E. Babusikova, J. Lehotsky, and D. Dobrota. 2003. Free radical-induced protein modification and inhibition of Ca2+-ATPase of cardiac sarcoplasmic reticulum. *Mol. Cell. Biochem.* 248:41–47. doi:10.1023/A:1024145212616

Khan, W.N. 2009. B cell receptor and BAFF receptor signaling regulation of B cell homeostasis. *J. Immunol.* 183:3561–3567. doi:10.4049/jimmunol.0800933

Kirichok, Y., G. Krapivinsky, and D.E. Clapham. 2004. The mitochondrial calcium uniporter is a highly selective ion channel. *Nature.* 427:360–364. doi:10.1038/nature02246

Leslie, C.C. 1997. Properties and regulation of cytosolic phospholipase A2. *J. Biol. Chem.* 272:16709–16712. doi:10.1074/jbc.272.27.16709

Liou, J., M.L. Kim, W.D. Heo, J.T. Jones, J.W. Myers, J.E. Ferrell Jr., and T. Meyer. 2005. STIM is a Ca2+ sensor essential for Ca2+-store-depletion-triggered Ca2+ influx. *Curr. Biol.* 15:1235–1241. doi:10.1016/j.cub.2005.05.055

Luik, R.M., M.M. Wu, J. Buchanan, and R.S. Lewis. 2006. The elementary unit of store-operated Ca^{2+} entry: local activation of CRAC channels by STIM1 at ER–plasma membrane junctions. *J. Cell Biol.* 174:815–825. doi:10.1083/jcb.200604015

Luik, R.M., B. Wang, M. Prakriya, M.M. Wu, and R.S. Lewis. 2008. Oligomerization of STIM1 couples ER calcium depletion to CRAC channel activation. *Nature.* 454:538–542. doi:10.1038/nature07065

Madesh, M., O. Benard, and K.A. Balasubramanian. 1998. Glutathione modulates lipid composition of human colon derived HT-29 cells. *Int. J. Biochem. Cell Biol.* 30:1345–1352. doi:10.1016/S1357-2725(98)00097-1

Madesh, M., B.J. Hawkins, T. Milovanova, C.D. Bhanumathy, S.K. Joseph, S.P. Ramachandrarao, K. Sharma, T. Kurosaki, and A.B. Fisher. 2005. Selective role for superoxide in $InsP_3$ receptor–mediated mitochondrial dysfunction and endothelial apoptosis. *J. Cell Biol.* 170:1079–1090. doi:10.1083/jcb.200505022

Minguet, S., E.P. Dopfer, C. Pollmer, M.A. Freudenberg, C. Galanos, M. Reth, M. Huber, and W.W. Schamel. 2008. Enhanced B-cell activation mediated by TLR4 and BCR crosstalk. *Eur. J. Immunol.* 38:2475–2487. doi:10.1002/eji.200738094

Parekh, A.B. 2008. Mitochondrial regulation of store-operated CRAC channels. *Cell Calcium.* 44:6–13. doi:10.1016/j.ceca.2007.12.006

Parekh, A.B., and J.W. Putney Jr. 2005. Store-operated calcium channels. *Physiol. Rev.* 85:757–810. doi:10.1152/physrev.00057.2003

Park, H.S., H.Y. Jung, E.Y. Park, J. Kim, W.J. Lee, and Y.S. Bae. 2004. Cutting edge: direct interaction of TLR4 with NAD(P)H oxidase 4 isozyme is essential for lipopolysaccharide-induced production of reactive oxygen species and activation of NF-kappa B. *J. Immunol.* 173:3589–3593.

Park, C.Y., P.J. Hoover, F.M. Mullins, P. Bachhawat, E.D. Covington, S. Raunser, T. Walz, K.C. Garcia, R.E. Dolmetsch, and R.S. Lewis. 2009. STIM1 clusters and activates CRAC channels via direct binding of a cytosolic domain to Orai1. *Cell.* 136:876–890. doi:10.1016/j.cell.2009.02.014

Pinton, P., C. Giorgi, R. Siviero, E. Zecchini, and R. Rizzuto. 2008. Calcium and apoptosis: ER-mitochondria Ca2+ transfer in the control of apoptosis. *Oncogene.* 27:6407–6418. doi:10.1038/onc.2008.308

Prakriya, M., S. Feske, Y. Gwack, S. Srikanth, A. Rao, and P.G. Hogan. 2006. Orai1 is an essential pore subunit of the CRAC channel. *Nature.* 443:230–233. doi:10.1038/nature05122

Qiu, H., A.S. Johansson, M. Sjöström, M. Wan, O. Schröder, J. Palmblad, and J.Z. Haeggström. 2006. Differential induction of BLT receptor expression on human endothelial cells by lipopolysaccharide, cytokines, and leukotriene B4. *Proc. Natl. Acad. Sci. USA.* 103:6913–6918. doi:10.1073/pnas.0602208103

Queiroga, C.S., A.S. Almeida, C. Martel, C. Brenner, P.M. Alves, and H.L. Vieira. 2010. Glutathionylation of adenine nucleotide translocase induced by carbon monoxide prevents mitochondrial membrane permeabilization and apoptosis. *J. Biol. Chem.* 285:17077–17088. doi:10.1074/jbc.M109.065052

Rizzuto, R., P. Pinton, W. Carrington, F.S. Fay, K.E. Fogarty, L.M. Lifshitz, R.A. Tuft, and T. Pozzan. 1998. Close contacts with the endoplasmic reticulum as determinants of mitochondrial Ca2+ responses. *Science.* 280:1763–1766. doi:10.1126/science.280.5370.1763

Roos, J., P.J. DiGregorio, A.V. Yeromin, K. Ohlsen, M. Lioudyno, S. Zhang, O. Safrina, J.A. Kozak, S.L. Wagner, M.D. Cahalan, et al. 2005. STIM1, an essential and conserved component of store-operated Ca^{2+} channel function. *J. Cell Biol.* 169:435–445. doi:10.1083/jcb.200502019

Ruprecht, C.R., and A. Lanzavecchia. 2006. Toll-like receptor stimulation as a third signal required for activation of human naive B cells. *Eur. J. Immunol.* 36:810–816. doi:10.1002/eji.200535744

Smyth, J.T., W.I. DeHaven, G.S. Bird, and J.W. Putney Jr. 2007. Role of the microtubule cytoskeleton in the function of the store-operated Ca2+ channel activator STIM1. *J. Cell Sci.* 120:3762–3771. doi:10.1242/jcs.015735

Smyth, J.T., W.I. Dehaven, G.S. Bird, and J.W. Putney Jr. 2008. Ca2+-store-dependent and -independent reversal of Stim1 localization and function. *J. Cell Sci.* 121:762–772. doi:10.1242/jcs.023903

Stathopulos, P.B., L. Zheng, G.Y. Li, M.J. Plevin, and M. Ikura. 2008. Structural and mechanistic insights into STIM1-mediated initiation of store-operated calcium entry. *Cell.* 135:110–122. doi:10.1016/j.cell.2008.08.006

Takata, M., Y. Homma, and T. Kurosaki. 1995. Requirement of phospholipase C-gamma 2 activation in surface immunoglobulin M-induced B cell apoptosis. *J. Exp. Med.* 182:907–914. doi:10.1084/jem.182.4.907

Taylor, E.R., F. Hurrell, R.J. Shannon, T.K. Lin, J. Hirst, and M.P. Murphy. 2003. Reversible glutathionylation of complex I increases mitochondrial superoxide formation. *J. Biol. Chem.* 278:19603–19610. doi:10.1074/jbc.M209359200

Veal, E.A., A.M. Day, and B.A. Morgan. 2007. Hydrogen peroxide sensing and signaling. *Mol. Cell.* 26:1–14. doi:10.1016/j.molcel.2007.03.016

Vig, M., C. Peinelt, A. Beck, D.L. Koomoa, D. Rabah, M. Koblan-Huberson, S. Kraft, H. Turner, A. Fleig, R. Penner, and J.P. Kinet. 2006. CRACM1 is a plasma membrane protein essential for store-operated Ca2+ entry. *Science.* 312:1220–1223. doi:10.1126/science.1127883

White, C., C. Li, J. Yang, N.B. Petrenko, M. Madesh, C.B. Thompson, and J.K. Foskett. 2005. The endoplasmic reticulum gateway to apoptosis by Bcl-X(L) modulation of the InsP3R. *Nat. Cell Biol.* 7:1021–1028. doi:10.1038/ncb1302

Yeromin, A.V., S.L. Zhang, W. Jiang, Y. Yu, O. Safrina, and M.D. Cahalan. 2006. Molecular identification of the CRAC channel by altered ion selectivity in a mutant of Orai. *Nature.* 443:226–229. doi:10.1038/nature05108

Yuan, J.P., W. Zeng, M.R. Dorwart, Y.J. Choi, P.F. Worley, and S. Muallem. 2009. SOAR and the polybasic STIM1 domains gate and regulate Orai channels. *Nat. Cell Biol.* 11:337–343. doi:10.1038/ncb1842

Zanoni, I., R. Ostuni, G. Capuano, M. Collini, M. Caccia, A.E. Ronchi, M. Rocchetti, F. Mingozzi, M. Foti, G. Chirico, et al. 2009. CD14 regulates the dendritic cell life cycle after LPS exposure through NFAT activation. *Nature.* 460:264–268. doi:10.1038/nature08118

Zhang, S.L., Y. Yu, J. Roos, J.A. Kozak, T.J. Deerinck, M.H. Ellisman, K.A. Stauderman, and M.D. Cahalan. 2005. STIM1 is a Ca2+ sensor that activates CRAC channels and migrates from the Ca2+ store to the plasma membrane. *Nature.* 437:902–905. doi:10.1038/nature04147